environmental microbiology

Environmental Microbiology (2021) **23**(8), 4505–4517 doi:10.1111/1462-2920.15643

Biochemistry of methanol-dependent acetogenesis in *Eubacterium callanderi* KIST612

Helge M. Dietrich, Florian Kremp, Christian Öppinger, Luna Ribaric and Volker Müller *

Department of Molecular Microbiology & Bioenergetics, Institute of Molecular Biosciences, Johann Wolfgang Goethe University, Max-von-Laue Str. 9, Frankfurt, D-60438, Germany.

Summary

Methanol is the simplest of all alcohols, is universally distributed in anoxic sediments as a result of plant material decomposition and is constantly attracting attention as an interesting substrate for anaerobes like acetogens that can convert bio-renewable methanol into value-added chemicals. A major drawback in the development of environmentally friendly but economically attractive biotechnological processes is the present lack of information on biochemistry and bioenergetics during methanol conversion in these bacteria. The mesophilic acetogen *Eubacterium callanderi* KIST612 is naturally able to consume methanol and produce acetate as well as butyrate. To grasp the full potential of methanol-based production of chemicals, we analysed the genes and enzymes involved in methanol conversion to acetate and identified the redox carriers involved. We will display a complete model for methanol-derived acetogenesis and butyrogenesis in *Eubacterium callanderi* KIST612, tracing the electron transfer routes and shed light on the bioenergetics during the process.

Introduction

Acetogenic bacteria are a phylogenetically diverse but nutritionally rather uniform group of strictly anaerobic bacteria (Schuchmann and Müller, 2016). They are characterized by a two-branched linear pathway for acetate formation from two mol of CO_2, the acetyl-CoA or Wood-Ljungdahl pathway (WLP) (Wood and Ljungdahl, 1991). The WLP is considered as an ancient pathway of CO_2 fixation since it is the only of currently seven known pathways for CO_2 fixation that is energy neutral (Calvin, 1962; Evans *et al*., 1966; Holo, 1989; Wood and Ljungdahl, 1991; Berg *et al*., 2007; Huber *et al*., 2008; Zarzycki *et al*., 2009; Sánchez-Andrea *et al*., 2020). In the methyl branch, one mol of CO_2 is reduced to formate that is then bound at the expense of ATP hydrolysis to the C_1 carrier tetrahydrofolate (THF). Formyl-THF is dehydrated to methenyl-THF and then reduced *via* methylene- to methyl-THF. The methyl group is the precursor of the methyl group of acetate and is transferred to the key enzyme of the pathway, the carbon monoxide dehydrogenase/acetyl-CoA synthase (CODH/ACS). A second molecule of CO_2 is reduced by the CODH, also bound to the CODH/ACS and serves as carbonyl group of acetate. CODH/ACS forms the carbon–carbon bond and introduces CoA into the molecule. Acetyl-CoA is then converted *via* acetyl phosphate to ATP and acetate (Andreesen *et al*., 1973).

Since the pathway reduces CO_2 *via* three two-electron reductions to a methyl group, the pathway is well suited to also accept other C1 substrates, such as formate, formaldehyde, carbon monoxide or methanol. Nearly all of these are highly interesting substrates for the production of value-added compounds in biotechnological processes. $H_2 + CO_2 + CO$ (synthesis gas, syngas) is already used in an industrial process as feedstock to produce ethanol, catalysed by *Clostridium autoethanogenum* (Norman *et al*., 2018). Methanol is another interesting feedstock that is currently synthesized at industrial large scale from syngas or methane, but can also be synthesized from coal, biomass or municipal solid waste (www.methanol.org/the-methanol-industry; Iaquaniello *et al*., 2017; Giuliano *et al*., 2020). Although it has been known for a long time that acetogens grow on methanol (Bache and Pfennig, 1981), the analysis of the enzymes and redox carriers involved as well as the ATP yield is lagging behind (Kremp *et al*., 2018; Kremp and Müller, 2021). The knowledge of the ATP yield is of special importance since acetogens grow at the thermodynamic limit of life (Schuchmann and Müller, 2014). The ATP yield is typically only a fraction of an ATP, thus making the implementation of ATP-demanding pathways for the synthesis of value-added compounds very challenging. *Eubacterium callanderi*

Received 29 April, 2021; accepted 13 June, 2021. *For correspondence. E-mail vmueller@bio.uni-frankfurt.de; Tel. (+49) 69 79829507; Fax (+49) 69 79829306.

KIST612 (formerly *Eubacterium limosum* KIST612) is one of the interesting organisms to be used as methylotrophic organism for it can produce butyrate naturally not only from gaseous CO or synthesis gas but also from the liquid C_1 compound methanol (Chang *et al*., 1997; Jeong *et al*., 2015; Litty and Müller, 2021). However, since nothing is known about the enzymes catalysing acetogenesis from methanol and the redox carriers involved, the ATP yield could not be calculated. To fill this gap, we have purified and analysed all the redox enzymes of the WLP in *E. callanderi* KIST612 and determined the redox carriers entangled in the WLP. This enabled us to identify the entire biochemistry of acetyl-CoA formation and to determine the ATP yield.

Results and discussion

The methanol-specific methyl transferase system

The methyl groups are mobilized by a methyltransferase system that is comprised of three proteins containing two catalytic domains (Kremp and Müller, 2021). The methyltransferase I (MTI) abstracts the methyl group from the substrate and transfers it to the central cobalt atom of a corrinoid-cofactor, the corrinoid protein, CoP (Das *et al*., 2007; Visser *et al*., 2016; Kremp *et al*., 2018). From there, the methyl group is transferred by a methyltransferase II (MTII) to tetrahydrofolate (Visser *et al*., 2016; Kremp *et al*., 2018). Since corrinoids are highly reactive in their superreduced active state, they undergo spontaneous autooxidation leading to an inactivation of the CoP. To return the corrinoid cofactor to the active state, so-called activating enzymes use ferredoxin/flavodoxin to reductively activate the corrinoid protein (Dürichen *et al*., 2019; Kißling *et al*., 2020). MTI confers the substrate specificity and a BLAST search using the *Eubacterium limosum* MTI (MttB, WP_038351887.1; (Kountz *et al*., 2020)) as query showed that the genome of *E. callanderi* KIST612 encodes 32 different MTI enzymes (Table S1), underlining the importance of methyl groups as carbon and energy source for *E. callanderi* KIST612. Recently, Chen and colleagues (2016) heterologously produced and isolated a MT system from the closely related *Eubacterium limosum* ZL-II that was shown to be methanol-specific. Since the genome of *E. limosum* ZL-II had not been sequenced, the group of Chen *et al*. used the genome of *E. callanderi* KIST612 as a reference for genetic analysis. Therefore, the genes coding for this methanol-specific methyltransferase system are actually originating from *E. callanderi* KIST612 and the corresponding proteins were identified as methanol:corrinoid methyltransferase (MTI; allocated locus tag ELI_2003), corrinoid protein (CoP; ELI_2004), methyltetrahydrofolate:corrinoid/iron–sulfur protein methyltransferase (MTII; ELI_2005) and activating enzyme (AE; ELI_0370) (Fig. 1). These proteins are similar to the proteins encoded by locus tags Awo_c22760-Awo_c22740 of *Acetobacterium woodii* that showed the highest expression levels of all methyl transferase genes during *A. woodii* growth on methanol (Kremp *et al*., 2018). Moreover, ELI_2003-ELI_2005 were recently shown by a proteomics approach to be upregulated during growth on methanol (Kim *et al*., 2021). Therefore, the genes assigned as ELI_2003-ELI_2005 most likely encode the methanol-specific methyl transferase system of *E. callanderi* KIST612.

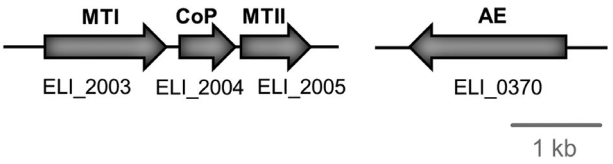

Fig. 1. Genetic organization of the putative methanol-specific methyltransferase system in *E. callanderi* KIST612. The potential operon consisting of ELI_2003 (coding for methyltransferase I, MTI), ELI_2004 (corrinoid protein, CP) and ELI_2005 (methyltransferase II, MTII) is located distinct from the activating enzyme (AE) encoded by ELI_0370. The activating enzyme acts on different corrinoid proteins.

The methylene-THF reductase is of the MetF/MetV type

Methyl-THF is oxidized to CO_2 (Equation 1) to gain six electrons for reduction of three mol CO_2 to CO. Since oxidation of methyl-THF yields only one mol of CO_2, but in the reductive part three mol CO_2 are needed (Equation (2)), two additional mol CO_2 are necessary in the displayed methanol conversion to acetate (Equation (3)), which are provided by the carbonate-buffered growth medium. Thus, methanol is converted according to:

$$1\,CH_3OH + 1\,H_2O \rightarrow 1\,CO_2 + 6e^- + 6H^+ \quad (1)$$

$$3CH_3OH + 3CO_2 + 6e^- + 6H^+ \rightarrow 3CH_3COOH + 3H_2O \quad (2)$$

$$4CH_3OH + 2\,CO_2 \rightarrow 3\,CH_3COOH + 2\,H_2O \quad (3)$$

Oxidation of the methyl group according to Equation (1) is the reversal of CO_2 reduction. The first enzyme in this process is the methylene-THF reductase. The redox couple methylene-THF/methyl-THF has a standard redox potential of $E_0' = -200$ mV (Wohlfarth and Diekert, 1991). Therefore, reduction of NAD^+ ($E_0' = -320$ mV) with methyl-THF as electron donor is highly endergonic ($\Delta G_0' = +23$ kJ/mol) and thus, the question is how the thermodynamic barrier is overcome. In *A. woodii*,

oxidation of methyl-THF and NAD^+ reduction by the purified methylene-THF reductase (MTHFR) is almost impossible (Kremp *et al*., 2018), unless the next enzyme, the methylene-THF dehydrogenase (MTHF-DH) is added to the enzyme (Bertsch *et al*., 2015). Obviously, the MTHF-DH removes the endproduct of the first reaction, thus energetically 'pulling' the methyl-THF-dependent NAD^+ reduction. Another solution to overcome the energetic barrier would be electron bifurcation (Li *et al*., 2008; Mock *et al*., 2014; Buckel and Thauer, 2018). The reduced low redox potential electron carrier ferredoxin (Fd, $E_0' = -500$ to -450 mV) could be oxidized with concomitant NAD^+ reduction in an exergonic reaction and thus 'drive' endergonic methylene-THF-dependent NAD^+ reduction, much like Fd_{red}-driven lactate oxidation in *A. woodii* by electron bifurcation/confurcation (Weghoff *et al*., 2015).

To address this question and investigate the biochemical properties of the enzyme, we purified the MTHFR from methanol-grown as well as from glucose-grown *E. callanderi* KIST612 using different chromatographic steps. MTHFR from cells grown on either substrate did not show any difference compared to each other. After the last purification step, the protein eluted in a single peak and was finally purified 150-fold from the cell-free crude extract (Table 1). The purified enzyme is a heterodimer of only two proteins with an apparent molecular mass of 33 kDa and 23 kDa, matching the expected MTHFR subunits MetF (32 kDa) and MetV (24 kDa) (Fig. 2A). Therefore, the MTHFR from *E. callanderi* KIST612 is of the MetVF type, as assumed by Jeong and colleagues (2015). The native size of the MetVF complex was analysed by size exclusion chromatography and amounted to be around 110 kDa (Fig. 2B), indicating a dimer consisting of two MetVF heterodimers. Whilst the enzyme performed methylene-THF-dependent oxidation of methylviologen (MV) with 644 U mg^{-1} and methyl-THF-dependent MV reduction with 31 U mg^{-1}, NAD(P)-dependent activity could neither be observed for methyl-THF oxidation nor for methylene-THF reduction (data not shown). However, the isolated enzyme

Table 1. Purification of the methylene-THF reductase (MTHFR) from *E. callanderi* KIST612.

Purification step	Protein (mg)	MTHFR activity (μmol min^{-1} mg^{-1})	Yield (%)	Purification (−fold)
Crude extract	2497.6	2.7	100.0	1.0
Cytoplasm	1871.7	3.3	100.7	1.2
Q-Sepharose	240.2	20.5	70.5	7.5
Phenyl-Sepharose	8.3	509.1	70.2	186.1
Superdex 200	5.5	579.6	55.4	211.9

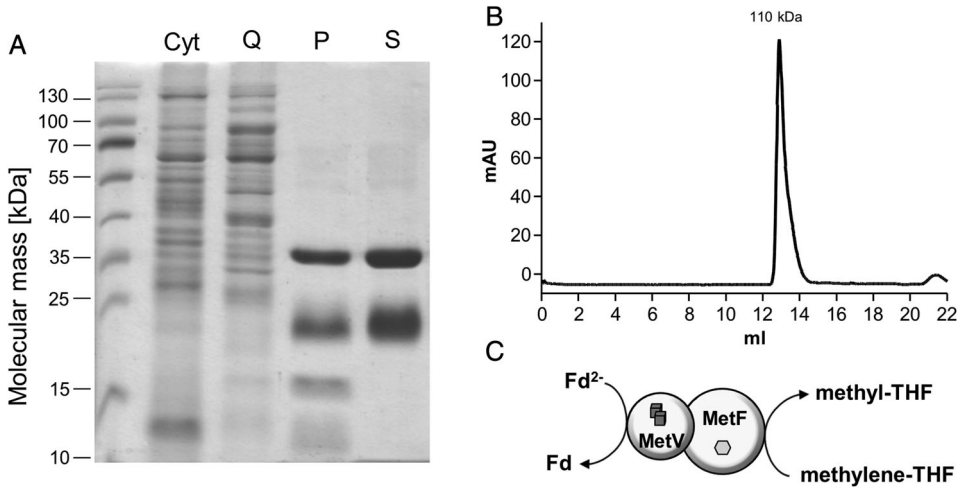

Fig. 2. Purification, determination of native size and hypothetical model of the methylene-THF reductase from *E. callanderi* KIST612.
A. 10 μg of cytoplasm and from the different purification steps Q-sepharose (Q), Phenyl-sepharose (P) and Superdex 200 (S) were separated by SDS-PAGE, following staining with Coomassie Brilliant Blue.
B. Separation of purified MTHFR (250 μg) on a Superdex 200 Increase 10/300 GL prepacked gel filtration column under anoxic conditions.
C. Model of the heterodimeric methylene-THF from *E. callanderi* KIST612. The hexagon represents protein-bound FMN, cubes represent iron–sulfur clusters.

showed methyl-THF production from methylene-THF and reduced Fd corresponding to an activity of 1.5 U mg^{-1} (Fig. 2C). Electron bifurcation or confurcation could not be observed using Fd and NAD^+ or $NADP^+$ as cofactors. Further characterization of basic enzymatic properties using MV as electron donor revealed a pH optimum at pH 6.0 and a temperature optimum at 40°C. After separation of the flavins from the purified MetVF by precipitation with trichloroacetic acid and applying the supernatant to a thin layer chromatography, FMN could be identified as the enzyme-bound flavin (1.1 ± 0.24 mol/heterodimer) which is in accordance with the MTHFRs from *Moorella thermoacetica* and *A. woodii* (Mock *et al*., 2014; Bertsch *et al*., 2015). Furthermore, the purified MTHFR contained 8.3 ± 0.95 and 8.4 ± 1 mol iron and sulfur per heterodimer, respectively which fits quite well to the predicted 2 [4Fe-4S] clusters in MetV (Fig. 2C).

The genes *metV* and *metF* are clustered together on the chromosome of *E. callanderi* KIST612. An overview of genetic organization of different methylene-THF reductase-encoding genes is given in the recent review by Kremp & Müller (2021). Contrary to *A. woodii* (Poehlein *et al*., 2012), there is no *rnfC2* gene next to *metV*/*metF* and nowhere else on the chromosome. RnfC2 confers NADH oxidation to the MetVF-type MTHFR in *A. woodii* (Bertsch *et al*., 2015). Unlike in *M. thermoacetica* (Mock *et al*., 2014), there are no *hdrCBA* genes next to *metVF*; in *M. thermoacetica* the presence of Hdr subunits in MTHFR is seen as possibility for the enzyme to use electron bifurcation to overcome the energetic barrier (Mock *et al*., 2014), but experimental evidence for this assumption is lacking. Concisely, the MTHFR of *E. callanderi* KIST612 is another example of a MetVF-type enzyme for which the natural electron donor remains to be established. *In vitro*, the enzyme does not use NAD(P) but reduced ferredoxin as electron donor (Clark and Ljungdahl, 1984; Wiechmann and Müller, 2021), but *in vivo*, this is questionable since energy would not be conserved but wasted and acetate formation from H_2+CO_2 would not be possible, but only possible for example from CO (Kremp & Müller, 2021).

The methylene-THF dehydrogenase is NAD^+ dependent

For a complete understanding of the bioenergetics during growth on methanol, it was important to investigate whether the methylene-THF dehydrogenase (MTHF-DH) is NAD^+ or $NADP^+$ specific. Therefore, cytoplasmic fractions of cells grown on methanol and harvested in late exponential growth phase were analysed for MTHF-DH activity. The cytoplasmic fraction catalysed methylene-THF oxidation with NAD^+ (9.78 U mg^{-1}) but not with $NADP^+$ (0.04 U mg^{-1}) as electron acceptor.

Formate dehydrogenase forms a complex with the bifurcating hydrogenase

The last step of the methyl group oxidation in the Wood-Ljungdahl pathway is the oxidation of formate to CO_2, as typically catalysed by formate dehydrogenases, but the electron carriers involved can be very different (Li *et al*., 1966; Schuchmann and Müller, 2013; Wang *et al*., 2013b; Wagner *et al*., 2016). Due to missing biochemical data for *E. callanderi* KIST612, Fd was mostly assumed as reaction partner of the formate dehydrogenase (Jeong *et al*., 2015; Kremp and Müller, 2021). To outline a reliable view of the biochemistry during growth on methanol and complete the picture of acetogenesis in *E. callanderi* KIST612, we purified the formate dehydrogenase from methanol-grown cells using three different chromatographic steps. Surprisingly, after each purification step the fractions containing formate dehydrogenase also showed hydrogenase activity. When the fractions were analysed for their protein content on SDS-polyacrylamide gels, proteins with molecular masses of 98, 65, 63 and 17 kDa were identified (Fig. 3A) that correspond in mass to FDH, HydB, HydA1 and HydC, respectively. The identity of these subunits as FDH, HydA1, HydB and HydC was verified by MALDI-TOF analysis (Fig. S1). The proteins of the FDH-Hyd complex were purified 52-fold (Hyd) and 60-fold (FDH) (Table 2). Compared to other bifurcating hydrogenases, the methylviologen-reducing activity of *E. callanderi* FDH-Hyd with H_2 is 2212 U mg^{-1} and is therefore in the range of other bifurcating hydrogenases (70–18,000 U mg^{-1}) (Kpebe *et al*., 2018).

Next, we analysed whether the isolated hydrogenase uses the mechanism of electron bifurcation. Indeed, the hydrogenase catalysed the simultaneous reduction of NAD^+ and Fd with H_2 as electron donor with activities of 1.5 U mg^{-1} for Fd reduction and 1.1 U mg^{-1} for NAD^+ reduction (Fig. 3), which is slightly lower than in *A. woodii* (3 U mg^{-1}) or other bifurcating hydrogenases (up to 60 U mg^{-1}) (Kpebe *et al*., 2018), but still in a range that would allow growth with hydrogen as electron source.

Next, we checked for electron bifurcation by the formate dehydrogenase. The purified protein showed coreduction of NAD^+ and Fd with formate (40 mM) as electron donor with a catalytic activity of 0.11 U mg^{-1} for reduction of ferredoxin and 0.10 U mg^{-1} for NAD^+ reduction. Reduction of either NAD^+ or Fd alone was neither observed with H_2 nor with formate as electron donor (data not shown). To determine flavins possibly bound to the enzyme, the purified enzyme was precipitated with trichloroacetic acid. After centrifugation, the flavin-containing supernatant was analysed by thin layer chromatography, depicting FMN as the flavin bound to the enzyme as it has been shown for other bifurcating formate dehydrogenases from *Gottschalkia acidurici* and *C. autoethanogenum* (Wang

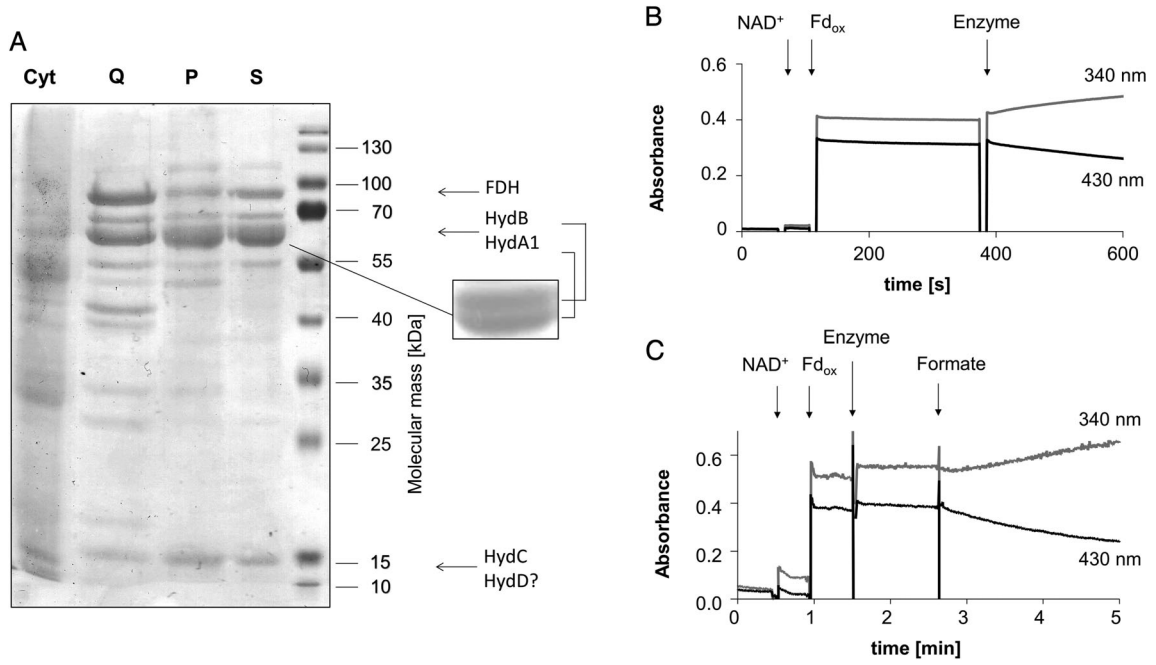

Fig. 3. Purification and activity of the electron-bifurcating hydrogenase in complex with the formate dehydrogenase from *E. callanderi* KIST612.
A. Samples of the different purification steps were separated by SDS-PAGE and stained with Coomassie Brilliant Blue. 30 μg of cytoplasm (Cyt) and 10 μg of pooled fractions from Q-sepharose (Q), pooled fractions from Phenyl-sepharose (P) and pooled fractions from Superdex 200 (S) were loaded onto the gel.
B. The purified bifurcating hydrogenase-formate dehydrogenase complex reduced NAD^+ (0.3 mM) and Fd (30 μM) at the same time, using H_2 (100% in the gas phase of the cuvette) as electron donor. NAD^+ and Fd reduction were monitored simultaneously at 430 nm (Fd reduction, $\varepsilon = 13.1\ mM^{-1}\ cm^{-1}$) and 340 nm ($NAD^+$ reduction, $\varepsilon = 6.3\ mM^{-1}\ cm^{-1}$).
C. Coupled reduction of NAD^+ and Fd, catalysed by purified bifurcating hydrogenase-formate dehydrogenase complex, but with formate (40 mM) as electron donor. All other reaction conditions are the same as in panel B.

Table 2. Purification of the electron-bifurcating hydrogenase and formate dehydrogenase from *E. callanderi* KIST612.

Purification step	Protein	Specific activity	Yield	Purification	Specific activity	Yield	Purification
		Hyd			FDH		
	(mg)	(μmol min^{-1} mg^{-1})	(%)	(−fold)	(μmol min^{-1} mg^{-1})	(%)	(−fold)
Crude extract	607.9	42.5	100.0	1.0	0.07	100.0	1.0
Cytoplasm	502.8	48.3	94.0	1.1	0.08	87.7	1.1
Q-Sepharose	67.8	331.2	86.9	7.8	0.47	71.4	6.4
Phenyl-Sepharose	8.0	1696.8	52.6	39.9	3.32	59.6	45.3
Superdex 200	4.4	2211.6	37.8	52.0	4.43	43.8	60.4

et al., 2013b; Wang *et al*., 2013a). Analysis of the temperature optimum of the enzyme showed that both catalytic subunits are most active between 35°C and 40°C. Increasing pH stimulated both formate dehydrogenase and hydrogenase activity, with the highest catalytic activities at pH 8.5 (FDH) and 10.5 (Hyd).

Formate dehydrogenase and bifurcating hydrogenase form a functional complex

An important question was whether both enzymes work together to reduce CO_2 with hydrogen as electron donor. Therefore, we followed the formate-dependent H_2 evolution as well as formate production from H_2 and CO_2. The purified enzyme was able to catalyse both reaction directions with a specific activity of 0.84 U mg^{-1} (H_2 evolution) and 30 mU mg^{-1} (formation of formate). Interestingly, the activities were significantly increased after addition of the cofactors NAD^+ and Fd (H_2 production: 2-fold to 1.82 U mg^{-1}; formate production: 3-fold to 100 mU mg^{-1}) before starting the reaction (Fig. 4). These results clearly show a direct functional connectivity of the catalytic subunits for the interconversion of formate and CO_2, but they also point out that (I) the reaction is strongly biased to formate oxidation and (II) the electron transfer between FDH and Hyd is more efficient if the

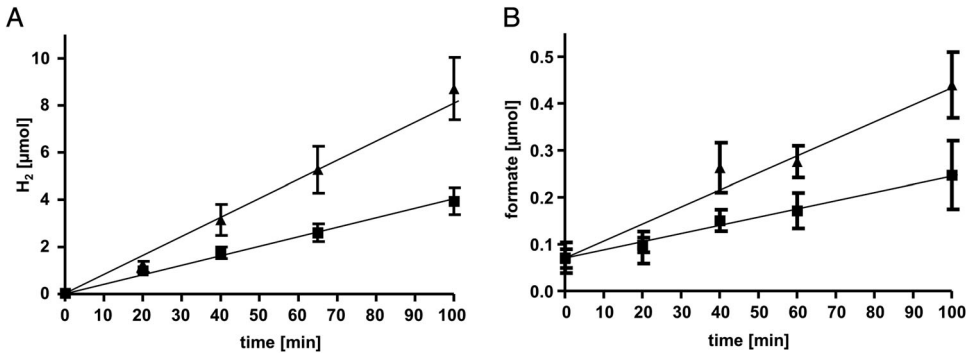

Fig. 4. The purified complex of formate dehydrogenase (FDH) and bifurcating hydrogenase (Hyd) catalyses H_2 evolution from formate as well as hydrogenation of CO_2 to formate.
A. Hydrogen formation from formate (150 mM) was performed by 40 µg isolated enzyme in buffer 6 (100 mM sodium phosphate, 2 mM DTE, 4 µM resazurin, pH 7.0) under an atmosphere of 100% N_2 at 37°C. The reaction was performed in presence (▲) and absence (■) of 0.3 mM NAD^+ and 30 µM Fd. H_2 was measured in the gas phase.
B. Formate production from H_2 and CO_2 was analysed as in panel A. but instead of formate, $H_2 + CO_2$ (80:20 [v/v], 1.1×10^5 Pa overpressure) in the gas phase was used as substrate. Again, catalysis was followed with (▲) and without (■) NAD^+ and Fd in the reaction buffer.

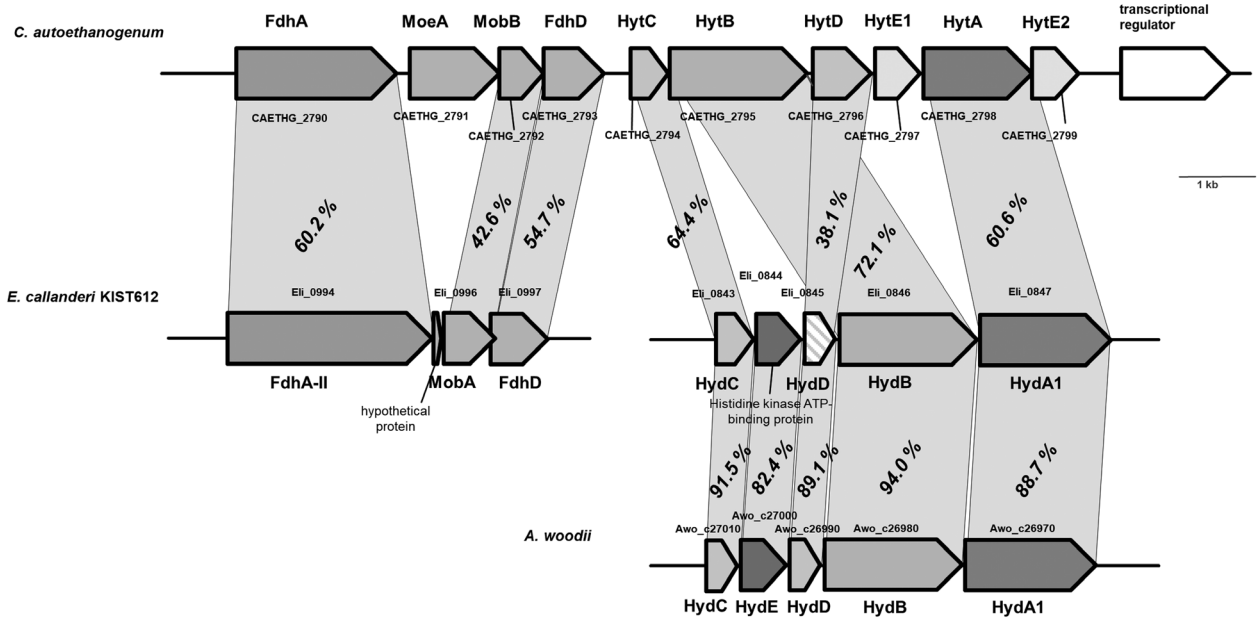

Fig. 5. Comparison of the genetic organizations of the FDH-Hyd complex genes in *C. autoethanogenum* and *E. callanderi* KIST612 as well as HydABCD genes in *A. woodii*. Genetic organization of the gene cluster of complex-forming formate dehydrogenase with the NADP- and ferredoxin-dependent bifurcating hydrogenase from *C. autoethanogenum* compared to the gene clusters encoding the genes for the FDH-Hyd complex in *E. callanderi* KIST612. Numbers show respective amino acid sequence similarities.

electrons are shuttled between the subunits by the soluble reduction equivalents NAD^+ and Fd. This is contrary to the FDH-Hyd complex from *C. autoethanogenum*, where both reaction directions are performed with the same efficiency and the addition of reducing equivalents did not increase the catalytic activity (Wang *et al*., 2013b).

Unlike the operon of the *C. autoethanogenum* FDH-Hyd complex (Wang *et al*., 2013b), the genes in *E. callanderi* KIST612 are divided in two separate gene clusters (Fig. 5). The formate dehydrogenase gene (ELI_0994) codes for FdhA-II and shows a high similarity to the *C. autoethanogenum* FdhA (CAETHG_2790, 60.2%). *fdhA-II* is located next to the genes *mobA* (ELI_0996) and *fdhD* (ELI_0997), which code for proteins involved in synthesis of the molybdopterin cofactor and formate dehydrogenase maturation, displaying a 42.6% and 54.7% similarity to the corresponding subunits from *C. autoethanogenum* (CAETHG_2792 & CAETHG_2793), respectively. As in other formate dehydrogenases, MobA and FdhD are not part of the active protein (Schuchmann and Müller, 2013; Wang *et al*., 2013b; Schwarz *et al*., 2018). The subunits of

the bifurcating hydrogenase are clustered together in a putative operon (ELI_0843-0847), which includes the genes coding for HydA1 (ELI_0847) harbouring the hydrogen-cluster, the putative flavin-containing and NAD-binding HydB (ELI_0846) and the electron-transferring HydC (ELI_0843). The produced proteins show high similarity (60%-72%) to the subunits of the FDH-Hyd complex of *C. autoethanogenum* (Wang *et al*., 2013b) but have a higher similarity to the subunits of the bifurcating hydrogenase HydABCD of *A. woodii* (89%-94%). The FDH-Hyd gene cluster in *C. autoethanogenum* furthermore encodes genes for MoeA (CAETHG_2791, involved in molybdopterin cofactor synthesis) as well as iron–sulfur cluster containing subunits HytE1 and HytE2 (CAETHG_2797 & CAETHG_2799; (Wang *et al*., 2013b)), which are altogether missing in the annotated *E. callanderi* gene cluster. In contrast, the *E. callanderi* KIST612 bifurcating hydrogenase gene cluster contains a gene annotated as a putative histidine kinase-like ATPase (ELI_0844) and iron–sulfur centre containing *hydD* (ELI_0845). However, neither HydD (38.1% similarity to *C. autoethanogenum* HytD, CAETHG_2796) nor the histidine kinase-like protein could be found in the isolated enzyme. Apart from the bifurcating hydrogenase described here, the genome of *E. callanderi* KIST612 encodes for a second, putative [FeFe] hydrogenase (ELI_2538) where the [FeS]-cluster coordinating cysteines as well as the H-cluster binding sites are conserved (Jeong *et al*., 2015). However, typical genes for additional interacting hydrogenase subunits are lacking in the genetic context of ELI_2538. The neighbouring genes include a thioredoxin-like [2Fe2S] ferredoxin (ELI_2537), two genes containing an ATC domain (ELI_2535) and a winged helix-turn-helix domain for DNA binding (ELI_2539), as well as two other genes with unknown function (ELI_2536, ELI_2540). Therefore, no hydrogenase function is hypothesized for ELI_2538. [NiFe] hydrogenases are not encoded in the *E. callanderi* KIST612 genome.

Conclusion

The overall reaction catalysed by the formate dehydrogenase/hydrogenase complex of *E. callanderi* KIST612 and *C. autoethanogenum* (Wang *et al*., 2013b; Mock *et al*., 2015) is identical. However, it may well be that ferredoxin and NAD^+ are essential electron carriers between the formate dehydrogenase and hydrogenase in *E. callanderi* KIST612 (Fig. 6) but this requires further in-depth biochemical analyses. Notably, *C. autoethanogenum* does not grow on methanol (Abrini *et al*., 1994) and the electron bifurcating formate dehydrogenase/hydrogenase complex of *E. callanderi* KIST612 may be an adaptation to enable growth on methanol. If hydrogen would be the end product during formate oxidation in methanol metabolization, it would have to be re-captured by another hydrogenase; such a hydrogen cycling was recently shown for *A. woodii* (Wiechmann *et al*., 2020). Typically, a membrane-bound hydrogenase would activate hydrogen and transfer electrons into an electron transport chain (Odom and Peck, 1984), thus leading to additional ATP synthesis by a chemiosmotic mechanism. This can be excluded since *E. callanderi* KIST612 does not encode additional hydrogenases. The same holds true for growth on CO (Fig. 7) that only yields reduced ferredoxin as electron donor for the WLP. Since there is no membrane-bound energy-converting hydrogenase (Ech) complex, ferredoxin must be used directly as electron donor for reduction of CO_2 to formate. However, it is conceivable that the enzyme may work as an emergency valve to release electrons as hydrogen in the presence of an electron imbalance as it has been proposed for the *C. autoethanogenum* FDH-Hyd complex (Wang *et al*., 2013b).

The methylene-THF dehydrogenase is NAD^+ dependent. In earlier studies, ATP synthase from methanol-grown cells and Rnf from cells grown on glucose were shown to be Na^+ dependent in *E. callanderi* KIST612 (Jeong *et al*., 2015; Litty and Müller, 2020). The Na^+ dependence of the Rnf could be verified with membranes isolated from cells grown on methanol (Fig. S2). The

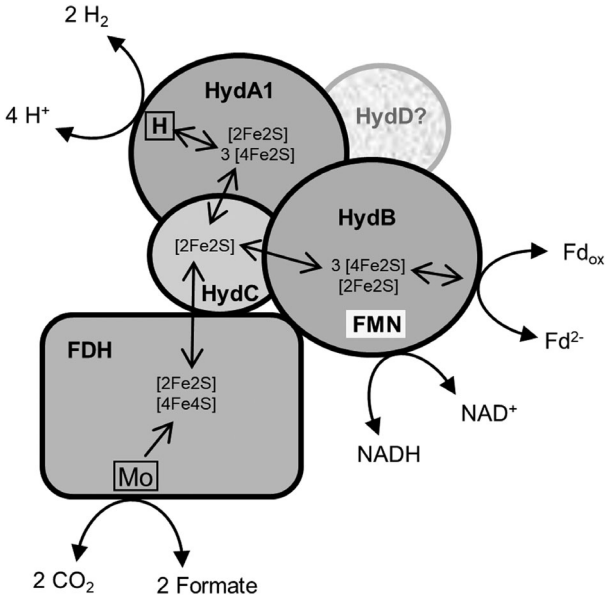

Fig. 6. Model of the electron bifurcating formate dehydrogenase-hydrogenase complex of *E. callanderi* KIST612. The FMN-containing bifurcating hydrogenase and the formate dehydrogenase from *E. callanderi* KIST612 form a complex that allows electron transfer either directly between the catalytic subunits *via* iron sulfur clusters or mediated by soluble cofactors NAD^+ and Fd. Whether HydD is part of the active complex remains unclear. Composition of iron–sulfur cofactors and FDH-bound metal ligand is based on sequence analysis. H, hydrogen cluster; Mo, molybdopterin cofactor; Fd_{ox}, oxidized ferredoxin; Fd^{2-}, reduced ferredoxin.

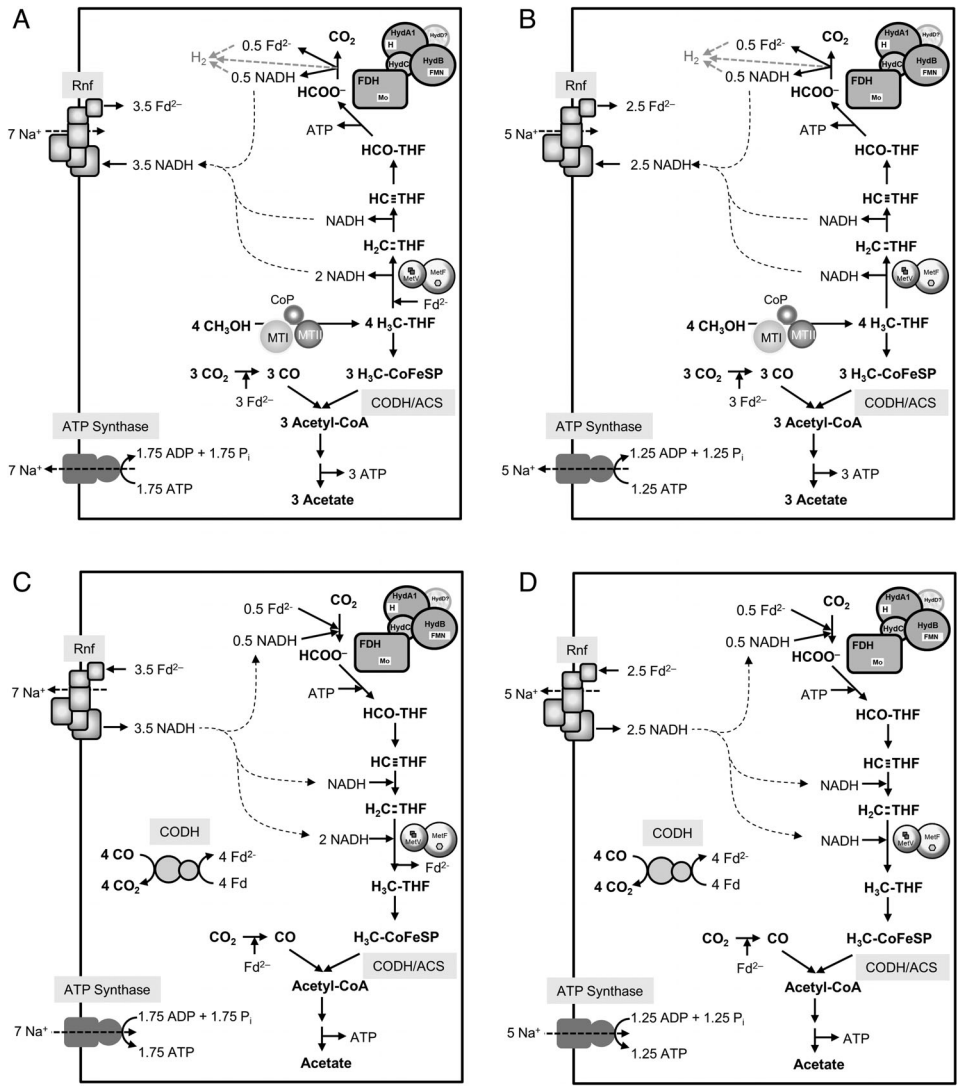

Fig. 7. Schematic overview of biochemistry and energy conservation during acetogenesis from methanol (A,B) or CO (C,D) in *E. callanderi* KIST612. Panel A and C depict models that include an electron bifurcating MTHFR, whereas the models in B and D do not have electron bifurcating MTHFR. NADH oxidation has never been demonstrated but could be conferred by a missing protein or the reductant is not a pyridine nucleotide but a compound with a similar redox potential. The stoichiometry of ions translocated per mol of ATP hydrolysed is unknown but is assumed to be 4. Hydrogen formation from formate seems unlikely, see text, and is therefore given in light grey. Fd, ferredoxin; THF, tetrahydrofolate; CoP, corrinoid protein; CoFeSP, corrinoid iron–sulfur protein; MTI, methyl transferase I; MTII, methyl transferase II; FDH, formate dehydrogenase; Hyd, hydrogenase subunits; Mo, molybdenum cofactor; H, hydrogen cluster.

methylene-THF reductase reaction remains enigmatic. *In vitro*, Fd^{2-} is used as reductant for methylene-THF reduction. If this would hold true *in vivo*, during growth on methanol Fd must be reduced in the course of methyl-THF oxidation. However, the energy barrier from methyl-THF to ferredoxin is even higher than to NAD, making Fd as oxidant highly unlikely, although the overall ATP yield would increase by 0.66 ATP. In contrast growth on $H_2 + CO_2$ would not be possible since the ATP yield would be negative with -0.3 ATP/acetate. Therefore, Fd can not be the electron carrier for the MTHFR *in vivo*. Therefore, we present two models for the biochemistry and bioenergetics of acetogenesis from methanol in *E. callanderi* KIST612. If we assume an electron bifurcating MTHFR (Fd-dependent NADH:methylene-THF oxidoreductase), the overall ATP yield during acetate production is 0.75 mol/mol acetate, whereas without an electron bifurcating MTHFR, the ATP yield is increased by 21% to 0.91 mol ATP/mol acetate. This is 264% more than the ATP yield from $H_2 + CO_2$ (0.25 ATP/acetate; (Jeong *et al*., 2015)) but 27% less ATP than during growth on CO (1.25 ATP/acetate, Fig. 7).

It has been reported before that under certain circumstances *E. callanderi* KIST612 naturally produces not only acetate but also butyrate (Jeong *et al*., 2015; Park *et al*., 2017; Litty and Müller, 2021). When butyrate is formed from methanol and the MTHFR is assumed to perform electron bifurcation, the ATP yield is 1.5 mol ATP/mol butyrate (Fig. 8A). Without an electron bifurcating MTHFR, this yield rises by 33% to 2 ATP/butyrate (Fig. 8B). During growth on CO, butyrate formation yields 4 ATP/butyrate (electron bifurcating MTHFR) or 3 ATP/butyrate (non-

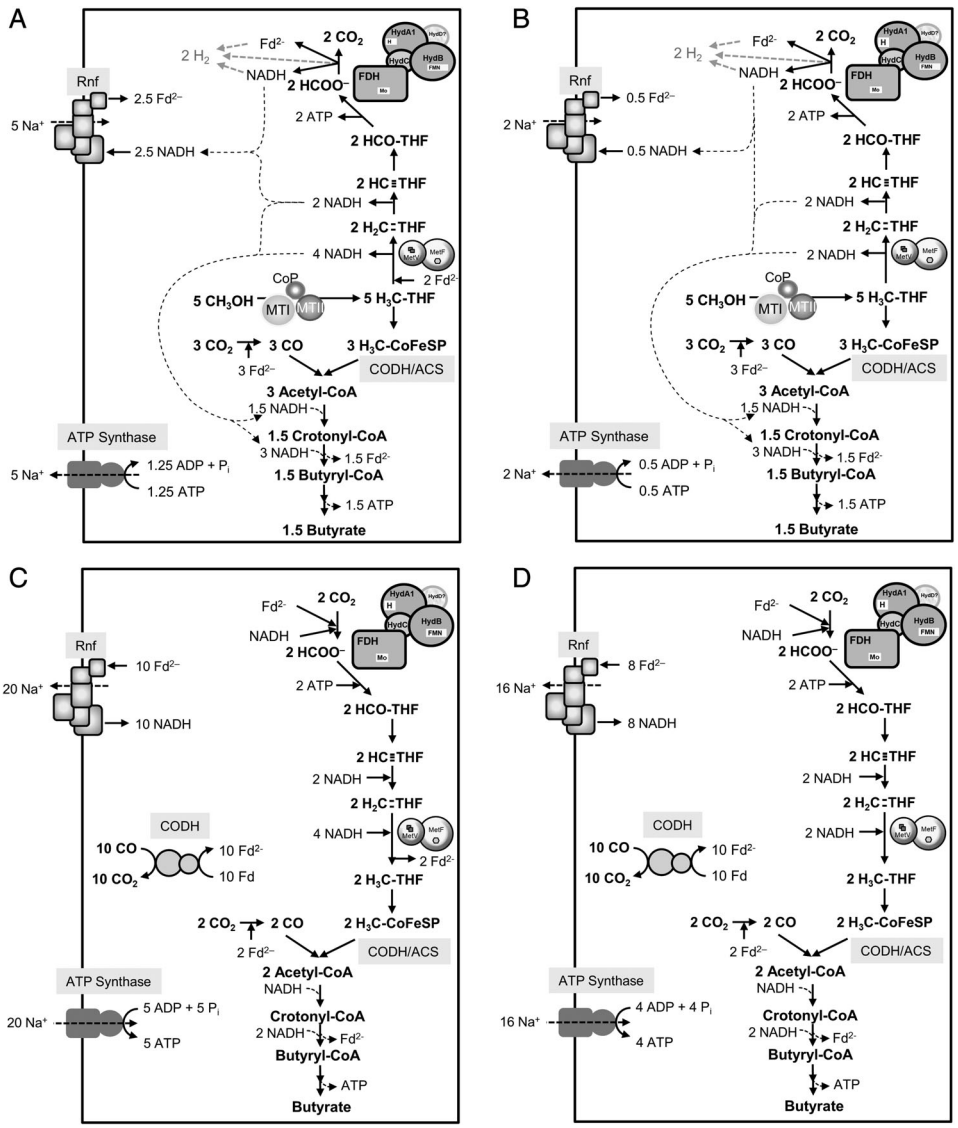

Fig. 8. Schematic overview of biochemistry and energy conservation during butyrogenesis from methanol (A,B) or CO (C,D) in *E. callanderi* KIST612. Panel A and C depict models that include an electron bifurcating MTHFR. NADH oxidation has never been demonstrated but could be conferred by a missing protein or the reductant is not a pyridine nucleotide but a compound with a similar redox potential. In contrast, the models in B and D do not have electron bifurcating MTHFR. The stoichiometry of ions translocated per mol of ATP hydrolysed is assumed to be 4. For abbreviations, see Fig. 7.

bifurcating MTHFR), respectively (Fig. 8C–D), which either way is a considerably higher ATP gain than from methanol or $H_2 + CO_2$ (1 mol ATP/butyrate, (Jeong *et al*., 2015)). With these data, the energetics of product formation from methanol can now be calculated.

Experimental procedures

Cultivation of E. callanderi *KIST612*

E. callanderi KIST612 was cultivated under strictly anoxic conditions in phosphate-buffered basal medium (PBBM) with 40 mM glucose or carbonate-buffered basal medium (CBBM) with 50 mM methanol as carbon and energy source at 37°C (Chang *et al*., 1999).

Cell harvest, membrane fraction isolation and cytosol preparation

All steps were performed under strictly anoxic conditions in an anaerobic chamber (Coy Laboratory Products, USA), filled with 96% N_2 and 4% H_2. Harvesting cells in late exponential stage, disruption of cells as well as membrane- and cytoplasm isolation was performed as described before (Jeong *et al*. 2015).

Gene analysis and comparison

Genetic analyses were performed using the Basic Local Alignment Search Tools (BLAST) from the National Center for Biotechnology Information (NCBI, Bethesda, MD,

USA [Wheeler *et al*., 2005]) and the Integrated Microbial Genomes and Microbiomes (IMG/M) data management and analysis system (Chen *et al*., 2021). For sequence comparisons, the Clustal Omega tool from the European Bioinformatics Institute (EMBL-EBI, Hinxton, UK) was used (Chojnacki *et al*., 2017).

Purification of the methylene-tetrahydrofolate reductase

Fifty millilitres of cytoplasm (38 mg ml^{-1} protein) isolated from 100 g wet cell mass was applied to a Q-Sepharose high-performance (HP) column (GE Healthcare, Chicago, IL, USA) equilibrated with buffer A (50 mM Tris–HCl, 20 mM $MgSO_4$, 20% glycerol, 2 mM DTE, 4 μM resazurin, pH 7.6) at a flow rate of 2 ml min^{-1}. Proteins were eluted using a linear NaCl gradient (0 to 500 mM) in buffer A at a flow rate of 1 ml min^{-1}. The pooled fractions showing methylene-THF-dependent reduction of methylviologen (MV) were incubated with ammonium sulfate to a concentration of 2 M and loaded onto a Phenyl-Sepharose HP column (GE Healthcare, Chicago, IL, USA) equilibrated with 2 M $(NH_4)_2SO_4$ at a flow rate of 1 ml min^{-1}. Proteins were eluted with a linear gradient of 2 to 0.6 M $(NH_4)_2SO_4$ at a flow rate of 1 ml min^{-1}. MTHFR-containing fractions were pooled and concentrated using 50-kDa Vivaspin ultrafiltration tubes (Sartorius Stedim Biotech GmbH, Germany). 500 μl of the concentrated protein was separated on a Superdex 200 10/300 GL prepacked column (GE Healthcare, Chicago, IL, USA) equilibrated with buffer A and eluted with a flow rate of 0.2 ml min^{-1}. The protein that eluted in a single peak was pooled and showed a 25-fold enrichment of MV:methylene-THF oxidoreductase activity compared to the cytosol, resulting in 1.8 mg of homogeneous protein that was stored at 4°C.

Purification of the formate dehydrogenase-hydrogenase complex

Cytoplasm from 25 g wet cell mass (31 ml, 16 mg ml^{-1}) was applied to a Q-Sepharose HP column (GE Healthcare, Chicago, IL, USA) equilibrated with buffer A (50 mM Tris–HCl, 20 mM $MgSO_4$, 20% glycerol, 2 mM DTE, 5 μM FMN, 4 μM resazurin, pH 7.2) at a flow rate of 1 ml min^{-1}. Protein was eluted with a linear gradient of 150 ml from 0 to 0.7 M NaCl in buffer A with a flow rate of 2 ml min^{-1}. Proteins showing formate-dependent MV reduction as well as hydrogen-dependent MV reduction eluted at 0.5 to 0.6 M NaCl and were pooled for further purification. 1.2 M $(NH_4)_2SO_4$ was added to the pooled fractions and the proteins were loaded on a Phenyl-Sepharose HP column (GE Healthcare, Chicago, IL, USA) equilibrated with 1.2 M $(NH_4)_2SO_4$ in buffer A at a flow rate of 1 ml min^{-1}. Proteins were eluted with a linear gradient of 1.2 to 0 M $(NH_4)_2SO_4$ with a flow rate of 1 ml min^{-1}. Formate- as well as hydrogen-dependent MV reduction activity eluted at around 0.12 to 0 M $(NH_4)_2SO_4$. The pooled fractions were concentrated by ultrafiltration using 50-kDa Vivaspin tubes (Sartorius Stedim Biotech GmbH, Germany). The concentrated sample was loaded on a Superdex 200 10/300 GL prepacked column (GE Healthcare, Chicago, IL, USA) equilibrated with buffer B (25 mM Tris–HCl, 150 mM NaCl, 20 mM $MgSO_4$, 20% glycerol, 2 mM DTE, 5 μM FMN, 4 μM resazurin, pH 7.5). Elution of the proteins was performed at a flow rate of 0.5 ml min^{-1}. Formate dehydrogenase as well as hydrogenase eluted together in two defined peaks from 8.5 ml to 12.5 ml. The pooled fractions were stored at 4°C.

Enzymatic assays

All enzyme assays, unless stated otherwise, were performed in 1.8 ml anoxic cuvettes (Glasgerätebau Ochs, Bovenden-Lenglern, Germany) sealed by rubber stoppers under a N_2 atmosphere at 37°C, with both enzyme and buffer pre-incubated at 37°C. Methylene-THF was synthesized non-enzymatically by mixing 1.5 mM formaldehyde with 0.5 mM THF (Sigma-Aldrich, Germany) in buffer 1 (50 mM potassium phosphate, 5 mM $MgCl_2$, 2 mM DTE, 4 μM resazurin, pH 7.0), leading to a racemic mixture of 0.25 mM methylene-THF (Wolfarth and Diekert, 1991; Sheppard *et al*. 1999).

Methylene-THF dependent oxidation of MV_{red} was measured in buffer 2 (50 mM MOPS, 10 mM NaCl, 20 mM $MgSO_4$, 2 mM DTE, 4 μM resazurin, pH 7.0). MV (5 mM) was added and prereduced to an A_{604} of ∼2, whereupon the reaction was started by addition of the protein.

Methyl-THF oxidation was measured as described earlier (Mock *et al*., 2014) but using MV as electron acceptor in buffer 3 (50 mM glycylglycine, 10 mM NaCl, 20 mM $MgSO_4$).

For MTHFR-mediated Fd_{red}-dependent methyl-THF production, Fd was purified and prereduced as described earlier (Schönheit *et al*., 1978; Kremp *et al*., 2020) and methylene-THF was reduced in 50 mM potassium phosphate (Kp_i) buffer (pH 7) after addition of purified MTHFR. After the reaction was stopped, proteins were removed using ultrafiltration in 3-kDa Vivaspin tubes. The flow through was analysed by HPLC on a Nucleopur RP C18 Gravity-SB column (MACHERY-NAGEL; particle size 3 μm, 150 mm by 4.6 mm) using an isocratic elution with 33 mM Kp_i buffer (pH 3) containing 7% of acetonitrile at a flow rate of 0.8 ml min^{-1} at 30°C. Methyl-THF was detected by measuring the absorbance at 313 nm.

Methylene-THF dehydrogenase (MTHF-DH), formate dehydrogenase (FDH), hydrogenase (HYD) and Rnf

activities were generally determined as described before (Bertsch *et al*., 2015; Jeong *et al*., 2015; Schwarz *et al*., 2018). Hydrogenase activity was measured in buffer 4 (50 mM CAPS, 2 mM DTE, 4 μM resazurin, pH 10.5), formate dehydrogenase was analysed in buffer 5 (50 mM EPPS, 2 mM DTE, 4 μM resazurin, pH 8.5). Hydrogen formation from formate and CO_2 reduction with H_2 to formate was performed in buffer 6 (100 mM sodium phosphate, 2 mM DTE, 4 μM resazurin, pH 7.0) in presence as well as in absence of 0.3 mM NAD^+ ($\varepsilon = 6.3\ mM^{-1}\ cm^{-1}$) and 30 μM *Clostridium pasteurianum*-ferredoxin ($\varepsilon = 13.1\ mM^{-1}\ cm^{-1}$) in the reaction mixture.

The coupled reduction of NAD^+ (0.3 mM) and ferredoxin from *C. pasteurianum* (30 μM) was analysed in buffer 6 with 10 μg of the isolated FDH-Hyd protein, using 40 mM formate or 100% H_2 in the gas phase (1.1×10^5 Pa overpressure) as electron donor.

Analytical methods

Quantification of protein concentration was performed according to the method of Bradford (1976). Protein separation was conducted in 12% SDS-polyacrylamide gels following staining with Coomassie brilliant blue G250. Determination of flavin content in purified proteins was performed as reported in Bertsch and colleagues (2013), with FAD and FMN as standards. The iron and sulfur content of the MTHFR was determined using colorimetrical methods of Fish (1988) and Beinert (1983). Calibration of the Superdex 200 10/300 GL prepacked gelfiltration column (GE Healthcare Life Sciences, Little Chalfont, UK) for size determination of the MTHFR was performed with Ferritin, Aldolase, Conalbumin and Ovalbumin (GE Healthcare Life Sciences, Little Chalfont, UK) as size standards in buffer B without FMN.

Acknowledgement

Financial support by the European Research Area Cofund on BioTechnologies (ERA CoBioTech; project BIOMETCHEM) is gratefully acknowledged.

Conflict of interest

The authors declare that they have no conflict of interest.

References

Abrini, J., Naveau, H., and Nyns, E.J. (1994) *Clostridium autoethanogenum*, sp. nov., an anaerobic bacterium that produces ethanol from carbon monoxide. *Arch Microbiol* **161**: 345–351.

Andreesen, J.R., Schaupp, A., Neurauter, C., Brown, A., and Ljungdahl, L.G. (1973) Fermentation of glucose, fructose, and xylose by *Clostridium thermoaceticum*: effect of metals on growth yield, enzymes, and the synthesis of acetate from CO_2. *J Bacteriol* **114**: 743–751.

Bache, R., and Pfennig, N. (1981) Selective isolation of *Acetobacterium woodii* on methoxylated aromatic acids and determination of growth yields. *Arch Microbiol* **130**: 255–261.

Beinert, H. (1983) Semi-micro methods for analysis of labile sulfide and of labile sulfide plus sulfane sulfur in unusually stable iron-sulfur proteins. *Anal Biochem* **131**: 373–378.

Berg, I.A., Kockelkorn, D., Buckel, W., and Fuchs, G. (2007) A 3-hydroxypropionate/4-hydroxybutyrate autotrophic carbon dioxide assimilation pathway in *Archaea*. *Science* **318**: 1782–1786.

Bertsch, J., Parthasarathy, A., Buckel, W., and Müller, V. (2013) An Electron-bifurcating Caffeyl-CoA Reductase. *J Biol Chem* **288**: 11304–11311.

Bertsch, J., Öppinger, C., Hess, V., Langer, J.D., and Müller, V. (2015) Heterotrimeric NADH-oxidizing methylenetetrahyd rofolate reductase from the acetogenic bacterium *Acetobacterium woodii*. *J Bacteriol* **197**: 1681–1689.

Bradford, M.M.(1976) A rapid and sensitive method for the quantification of microgram quantities of protein utilizing the principle of proteine-dye-binding. *Anal Biochem* **72**: 248–254.

Buckel, W., and Thauer, R.K. (2018) Flavin-based electron bifurcation, ferredoxin, flavodoxin, and anaerobic respiration with protons (Ech) or NAD^+ (Rnf) as electron acceptors: a historical review. *Front Microbiol* **9**: 401.

Calvin, M. (1962) The path of carbon in photosynthesis. *Science* **135**: 879–889.

Chang, I.S., Kim, B.H., Kim, D.H., Lovitt, R.W., and Sung, H. C. (1999) Formulation of defined media for carbon monoxide fermentation by *Eubacterium limosum* KIST612 and the growth characteristics of the bacterium. *J Biosci Bioeng* **88**: 682–685.

Chang, I.S., Kim, D.H., Kim, B.H., Shin, P.K., Yoon, J.H., Lee, J.S., and Park, Y.H. (1997) Isolation and identification of carbon monoxide utilizing anaerobe, *Eubacterium limosum* KIST612. *Kor J Appl Microbiol Biotechnol* **25**: 1–8.

Chen, I.A., Chu, K., Palaniappan, K., Ratner, A., Huang, J., Huntemann, M., *et al*. (2021) The IMG/M data management and analysis system v.6.0: new tools and advanced capabilities. *Nucleic Acids Res* **49**: D751–D763.

Chen, J.X., Deng, C.Y., Zhang, Y.T., Liu, Z.M., Wang, P.Z., Liu, S.L., *et al*. (2016) Cloning, expression, and characterization of a four-component O-demethylase from human intestinal bacterium *Eubacterium limosum* ZL-II. *Appl Microbiol Biotechnol* **100**: 9111–9124.

Chojnacki, S., Cowley, A., Lee, J., Foix, A., and Lopez, R. (2017) Programmatic access to bioinformatics tools from EMBL-EBI update: 2017. *Nucleic Acids Res* **45**: W550–W553.

Clark, J.E., and Ljungdahl, L.G. (1984) Purification and properties of 5,10-methylenetetrahydrofolate reductase, an iron-sulfur flavoprotein from *Clostridium formicoaceticum*. *J Biol Chem* **259**: 10845–10849.

Das, A., Fu, Z.Q., Tempel, W., Liu, Z.J., Chang, J., Chen, L., *et al*. (2007) Characterization of a corrinoid protein involved in the C1 metabolism of strict anaerobic bacterium *Moorella thermoacetica*. *Proteins* **67**: 167–176.

Dürichen, H., Diekert, G., and Studenik, S. (2019) Redox potential changes during ATP-dependent corrinoid reduction determined by redox titrations with europium(II)-DTPA. *Protein Sci* **28**: 1902–1908.

Evans, M.C., Buchanan, B.B., and Arnon, D.I. (1966) A new ferredoxin-dependent carbon reduction cycle in a photosynthetic bacterium. *Proc Natl Acad Sci U S A* **55**: 928–934.

Fish, W.W. (1988) Rapid colorimetric micromethod for the quantitation of complexed iron in biological samples. *Methods Enzymol* **158**: 357–364.

Giuliano, A., Freda, C., and Catizzone, E. (2020) Techno-economic assessment of bio-syngas poduction for methanol snthesis: a focus on the water-gas shift and carbon capture sections. *Bioengineering (Basel)* **7**: 70.

Holo, H. (1989) *Chloroflexus aurantiacus* secretes 3-hydroxypropionate, a possible intermediate in the assimilation of CO_2 and acetate. *Arch Microbiol* **151**: 252–256.

Huber, H., Gallenberger, M., Jahn, U., Eylert, E., Berg, I.A., Kockelkorn, D., *et al*. (2008) A dicarboxylate/4--hydroxybutyrate autotrophic carbon assimilation cycle in the hyperthermophilic Archaeum *Ignicoccus hospitalis*. *Proc Natl Acad Sci U S A* **105**: 7851–7856.

Iaquaniello, G., Centi, G., Salladini, A., Palo, E., Perathoner, S., and Spadaccini, L. (2017) Waste-to-methanol: process and economics assessment. *Bioresour Technol* **243**: 611–619.

Jeong, J., Bertsch, J., Hess, V., Choi, S., Choi, I.G., Chang, I.S., and Müller, V. (2015) Energy conservation model based on genomic and experimental analyses of a carbon monoxide-utilizing, butyrate-forming acetogen, *Eubacterium limosum* KIST612. *Appl Environ Microbiol* **81**: 4782–4790.

Kim, J.Y., Park, S., Jeong, J., Lee, M., Kang, B., Jang, S.H., *et al*. (2021) Methanol supply speeds up synthesis gas fermentation by methylotrophic-acetogenic bacterium, *Eubacterium limosum* KIST612. *Bioresour Technol* **321**: 124521.

Kißling, L., Greiser, Y., Dürichen, H., and Studenik, S. (2020) Flavodoxin hydroquinone provides electrons for the ATP-dependent reactivation of protein-bound corrinoid cofactors. *FEBS J* **287**: 4971–4981.

Kountz, D.J., Behrman, E.J., Zhang, L., and Krzycki, J.A. (2020) MtcB, a member of the MttB superfamily from the human gut acetogen *Eubacterium limosum*, is a cobalamin-dependent carnitine demethylase. *J Biol Chem* **295**: 11971–11981.

Kpebe, A., Benvenuti, M., Guendon, C., Rebai, A., Fernandez, V., Le Laz, S., *et al*. (2018) A new mechanistic model for an O_2-protected electron-bifurcating hydrogenase, Hnd from *Desulfovibrio fructosovorans*. *Biochim Biophys Acta Bioenerg* **1859**: 1302–1312.

Kremp, F., and Müller, V. (2021) Methanol and methyl group conversion in acetogenic bacteria: biochemistry, physiology and application. *FEMS Microbiol Rev* **45**: fuaa040.

Kremp, F., Roth, J., and Müller, V. (2020) The *Sporomusa* type Nfn is a novel type of electron-bifurcating transhydrogenase that links the redox pools in acetogenic bacteria. *Sci Rep* **10**: 14872.

Kremp, F., Poehlein, A., Daniel, R., and Müller, V. (2018) Methanol metabolism in the acetogenic bacterium *Acetobacterium woodii*. *Environ Microbiol* **20**: 4369–4384.

Li, F., Hinderberger, J., Seedorf, H., Zhang, J., Buckel, W., and Thauer, R.K. (2008) Coupled ferredoxin and crotonyl coenzyme A (CoA) reduction with NADH catalyzed by the butyryl-CoA dehydrogenase/Etf complex from *Clostridium kluyveri*. *J Bacteriol* **190**: 843–850.

Li, L.F., Ljungdahl, L., and Wood, H.G. (1966) Properties of nicotinamide adenine dinucleotide phosphate-dependent formate dehydrogenase from *Clostridium thermoaceticum*. *J Bacteriol* **92**: 405–412.

Litty, D., and Müller, V. (2020) A $Na+$ A1AO ATP synthase with a V-type c subunit in a mesophilic bacterium. *FEBS J* **287**: 3012–3023.

Litty, D., and Müller, V. (2021) Butyrate production in the acetogen *Eubacterium limosum* is dependent on the carbon and energy source. *Microb Biotechnol*. http://dx.doi.org/10.1111/1751-7915.13779.

Mock, J., Wang, S., Huang, H., Kahnt, J., and Thauer, R.K. (2014) Evidence for a hexaheteromeric methylenetetrahydrofolate reductase in *Moorella thermoacetica*. *J Bacteriol* **196**: 3303–3314.

Mock, J., Zheng, Y., Mueller, A.P., Ly, S., Tran, L., Segovia, S., *et al*. (2015) Energy conservation associated with ethanol formation from H_2 and CO_2 in *Clostridium autoethanogenum* involving electron bifurcation. *J Bacteriol* **197**: 2965–2980.

Norman, R.O.J., Millat, T., Winzer, K., Minton, N.P., and Hodgman, C. (2018) Progress towards platform chemical production using *Clostridium autoethanogenum*. *Biochem Soc Trans* **46**: 523–535.

Odom, J.M., and Peck, H.D., Jr. (1984) Hydrogenase, electron-transfer proteins, and energy coupling in the sulfate-reducing bacteria *Desulfovibrio*. *Annu Rev Microbiol* **38**: 551–592.

Park, S., Yasin, M., Jeong, J., Cha, M., Kang, H., Jang, N., *et al*. (2017) Acetate-assisted increase of butyrate production by *Eubacterium limosum* KIST612 during carbon monoxide fermentation. *Bioresour Technol* **245**: 560–566.

Poehlein, A., Schmidt, S., Kaster, A.-K., Goenrich, M., Vollmers, J., Thürmer, A., *et al*. (2012) An ancient pathway combining carbon dioxide fixation with the generation and utilization of a sodium ion gradient for ATP synthesis. *PLoS One* **7**: e33439.

Sánchez-Andrea, I., Guedes, I.A., Hornung, B., Boeren, S., Lawson, C.E., Sousa, D.Z., *et al*. (2020) The reductive glycine pathway allows autotrophic growth of *Desulfovibrio desulfuricans*. *Nat Commun* **11**: 5090.

Schönheit, P., Wäscher, C., and Thauer, R.K. (1978) A rapid procedure for the purification of ferredoxin from *Clostridia* using polyethylenimine. *FEBS Lett* **89**: 219–222.

Schuchmann, K., and Müller, V. (2013) Direct and reversible hydrogenation of CO_2 to formate by a bacterial carbon dioxide reductase. *Science* **342**: 1382–1385.

Schuchmann, K., and Müller, V. (2014) Autotrophy at the thermodynamic limit of life: a model for energy conservation in acetogenic bacteria. *Nat Rev Microbiol* **12**: 809–821.

Schuchmann, K., and Müller, V. (2016) Energetics and application of heterotrophy in acetogenic bacteria. *Appl Environ Microbiol* **82**: 4056–4069.

Schwarz, F.M., Schuchmann, K., and Müller, V. (2018) Hydrogenation of CO_2 at ambient pressure catalyzed by a highly active thermostable biocatalyst. *Biotechnol Biofuels* **11**: 237.

Sheppard, C. A., Trimmer, E. E., and Matthews, R. G. (1999) Purification and Properties of NADH-Dependent 5,10-methylenetetrahydrofolate reductase (MetF) from Escherichia coli. *J Bacteriol* **181**: 718–725.

Visser, M., Pieterse, M.M., Pinkse, M.W., Nijsse, B., Verhaert, P.D., de Vos, W.M., *et al*. (2016) Unravelling the one-carbon metabolism of the acetogen *Sporomusa* strain An4 by genome and proteome analysis. *Environ Microbiol* **18**: 2843–2855.

Wagner, T., Ermler, U., and Shima, S. (2016) The methanogenic CO_2 reducing-and-fixing enzyme is bifunctional and contains 46 [4Fe-4S] clusters. *Science* **354**: 114–117.

Wang, S., Huang, H., Kahnt, J., and Thauer, R.K. (2013a) *Clostridium acidurici* electron-bifurcating formate dehydrogenase. *App Environ Microbiol* **79**: 6176–6179.

Wang, S., Huang, H., Kahnt, J., Müller, A.P., Köpke, M., and Thauer, R.K. (2013b) NADP-specific electron-bifurcating [FeFe]-hydrogenase in a functional complex with formate dehydrogenase in *Clostridium autoethanogenum* grown on CO. *J Bacteriol* **195**: 4373–4386.

Weghoff, M.C., Bertsch, J., and Müller, V. (2015) A novel mode of lactate metabolism in strictly anaerobic bacteria. *Environ Microbiol* **17**: 670–677.

Wheeler, D.L., Barrett, T., Benson, D.A., Braynt, S.H., Canese, K., Church, D.M., *et al*. (2005) Database resources of the National Center for Biotechnology Information. *Nucleic Acids Res* **33**(Database issue): D39–45.

Wiechmann, A., Ciurus, S., Oswald, F., Seiler, V.N., and Müller, V. (2020) It does not always take two to tango: "Syntrophy" *via* hydrogen cycling in one bacterial cell. *ISME J* **14**: 1561–1570.

Wiechmann, A., and Müller, V. (2021) Energy conservation in the acetogenic bacterium Clostridium aceticum. *Microorganisms* **9**: 258.

Wohlfarth, G., and Diekert, G. (1991) Thermodynamics of methylenetetrahydrofolate reduction to methyltetrahydrofolate and its implications for the energy metabolism of homoacetogenic bacteria. *Arch Microbiol* **155**: 378–381.

Wood, H.G., and Ljungdahl, L.G. (1991) Autotrophic character of the acetogenic bacteria. In *Variations in Autotrophic Life*, Shively, J.M., and Barton, L.L. (eds). San Diego: Academic press, pp. 201–250.

Zarzycki, J., Brecht, V., Müller, M., and Fuchs, G. (2009) Identifying the missing steps of the autotrophic 3-hydroxypropionate CO_2 fixation cycle in *Chloroflexus aurantiacus*. *Proc Natl Acad Sci U S A* **106**: 21317–21322.

Supporting Information

Additional Supporting Information may be found in the online version of this article at the publisher's web-site:

Fig. S1. Identification of the proteins of the FDH-Hyd complex from *E. callanderi* KIST612. A. 10 μg of the cytoplasm (Cyt) and different purification steps Q-sepharose (Q), Phenyl-sepharose (P) and Superdex 200 (S) were separated by SDS-PAGE, following staining with Coomassie Brilliant Blue. B. Results of protein identification by peptide mass fingerprinting and corresponding genes. C. Analysis of the amino acid sequence of FDH-Hyd subunits from *E. callanderi* KIST612. To analyse the amino acid sequence of each subunit, the proteins were excised from the gel shown in (A) and analysed by MALDI-TOF-MS. The identified amino acids are highlighted in yellow.

Fig. S2. Na^+-stimulated ferredoxin:NAD+ oxidoreductase activity in *E. callanderi* KIST612 membranes. 30 μM reduced Ferredoxin (Fd, reduced with CO dehydrogenase of *A. woodii* under 100% CO atmosphere) was used to reduce 1 mM NAD^+ with 140 μg membrane protein in 50 mM Tris, 2 mM DTE, pH 7.5. 5 mM NaCl stimulated the NAD^+ reduction (black solid line), whereas in the control no NaCl was added (grey dashed line). The contaminating Na^+ concentration of 0.1 mM allowed for residual Rnf activity.

Table S1. Genes of *Eubacterium callanderi* KIST612 annotated as methyltransferase I. *E. limosum* MTI (WP_038351887.1) was used as query, using the IMG database.